International Journal of Power Electronics and Drive Systems (IJPEDS)
Vol. 12, No. 3, September 2021, pp. 1369~1378
ISSN: 2088-8694, DOI: 10.11591/ijpeds.v12.i3.pp1369-1378

Online efficiency optimization of IPMSM for electric vehicles

Hanaa Elsherbiny, Mohamed Kamal Ahmed, Mahmoud A. Elwany
Department of Electrical Engineering, Faculty of Engineering, El-Azhar University, Cairo, Egypt

Article Info

Article history:

Received Mar 16, 2021
Revised Apr 30, 2021
Accepted May 9, 2021

Keywords:

Finite element analysis
Interior permanent magnet synchronous motors
Inverter and iron losses
Online efficiency optimization

ABSTRACT

This paper presents an online efficiency optimization method for the interior permanent magnet synchronous motor (IPMSM) drive system in an electric vehicle (EV). The proposed method considers accurately the total system losses including fundamental copper and iron losses, harmonic copper and iron losses, magnet loss, and inverter losses. Therefore, it has the capability to always guarantee maximum efficiency control. A highly trusted machine model is built using finite element analysis (FEA). This model considers accurately the magnetic saturation, spatial harmonics, and iron loss effect. The overall system efficiency is estimated online based on the accurate determination of system loss, and then the optimum current angle is defined online for the maximum efficiency per ampere (MEPA) control. A series of results is conducted to show the effectiveness and fidelity of proposed method. The results show the superior performance of proposed method over the conventional offline efficiency optimization methods.

Corresponding Author:

Hanaa Elsherbiny
Department of Electrical Engineering
El-Azhar University
El-Nasr Road, Nasr City, 11751 Cairo, Egypt
Email: Hanaaelsherbiny.60@azhar.edu.eg

1. INTRODUCTION

The electric vehicles (EVs) are the future of transportation. They have lots of advantages such as no emissions, low maintenance, low cost, and safety drive [1]-[3]. However, the batteries have limited capacities that affects the milage per charge. As most of battery power is consumed by the main drive system (motor + converter), it is very important to optimize their efficiencies to increase milage per battery charge.

At early days of transportation, the direct current machines (DCMs) were used because they have simple and linear controls. However, the existence of commutator and brushes cause lots of problems leading to lower speed ranges and lower efficiencies [4]. Recentely, due to the huge progress in field of power electronics and semi-conductors, the induction machines (IMs), synchronous reluctance machines (SynRMs), switched reluctance machines (SRMs), and interior permanent magnet synchronous machines (IPMSMs) are reported for EVs. Due to the presence of copper losses in IMs, they have relatively low efficiencies and low power factors which is disadvantageous for EV traction. The SynRMs have relatively high torque ripple. They also need high volt amper (VA) rating of inverters due to the poor power factor. The SRMs have hnherited high torque ripple due to the sequential commutation of coils, doubly salient structure, and deep magnetic saturation. They also poss complicated control algorithms [4]-[7]. The IPMSMs have the best performance to be used as the main drive in EVs. They offer not only high efficiency, wide speed range, high power density, but also small weight and size with low noise [8], [9]. Despite the high efficiency of the IPMSMs, much research has been conducted to improve motor efficiency. On one side, new design configurations for both the stator and rotor are developed to improve motor efficiency [5], [8]. Also, the converter design is investigated for better system efficiency [10], [11]. On the other side, new control

techniques are introduced to improve system efficiency. First, the maximum torque per ampere (MTPA) is developed [12]-[15]. Then, the maximum efficiency per ampere (MEPA) is introduced [16]-[20].

The MEPA has better efficiency improvement compared to MTPA. This is mainly because the MTPA control reduces only the copper losses in PMSM [17], [18]. As a result, it does not guarantee the maximum system efficiency (motor + converter). On the contrary, the MEPA considers not only the copper losses in PMSM but also the iron losses, inverter losses, mechanical losses, and harmonic iron and copper losses. This, in turn, helps to accurately estimate and improve the overall system efficiency [17]-[20]. Therefore, the MEPA control has an increasing interest by the research community. Ni *et al*., Uddin and Rebeiro, and Yang *et al*. in [18]-[20], the fundamental iron losses are considered to maximize the system efficiency. However, harmonic iron losses are not considered which affect motor efficiency, especially in the high-speed and light load regions [16]. Balamurali *et al* and Ni *et al*. in [16]-[18], offline MEPA control methods are proposed. These methods require numerous repetitive experiments to generate the lookuptables. The detailed information of machine losses under all operation conditions is also required. Moreover, they are very time-consuming and require a huge computation burden. Furthermore, the high frequency machine losses are rarely considered, which results in an inevitable searching error [21], [22]. In addition, the generated lookup table does not consider the variation of stator resistance due to temperature, the variation of DC voltage, and the variation of machine parameters. The lookup table fits only a limited area of operation. To solve these problems, an online maximum efficiency per ampere (OMEPA) control method has been developed in this paper.

This paper presents an OMEPA control method for IPMSM in EVs. First, an accurate machine model that considers magnetic saturation, spatial harmonics, and iron loss effect is built. The finite element analysis (FEA) is employed to calculate the magnetic characteristics of IPMSM. The FEA considers accurately the saturation and spatial harmonics as well as cross-coupling. Second, the total system efficiency is calculated accurately by the consideration of detailed system losses including fundamental and harmonic iron losses, copper losses, as well as inverter losses. Third, an online searching algorithm for MEPA has been developed to derive the optimal current angle, and hence the optimal efficiency over the entire speed range.

The rest of the paper is organized is being as: Section 2 involves the detailed system and loss modelling. Section 3 gives the proposed online MEPA control. The results and discussions are in Section 4. Finally, Section 5 is the conclusion.

2. SYSTEM MODELING

The system modeling involves the modelling of IPMSM and the detailed analysis of system losses including copper losses, fundamental iron losses, harmonic iron losses, magnet loss, and inverter losses.

2.1. Modeling of IPMSM

The modeling of an IPMSM can be represented by (1).

$$v_{d,q} = R_s i_{d,q} + \frac{d\lambda_{d,q}}{dt} - \omega_e \lambda_{q,d}, \quad T_e = \frac{3}{2} p i_q \left(\lambda_d i_q - \lambda_q i_d\right), \quad J\frac{d\omega}{dt} = T_e - T_L - B\omega \tag{1}$$

where (v_d, v_q), (i_d, i_q), and (λ_d, λ_q) are d and q-axis components of voltage, current, and flux-linkage, respectively. R_s is the stator resistance. ω_e and ω are the electrical and mechanical angular speeds. T_e is the motor torque, p is the pole pairs, J is the inertia, B is the frictional coefficient, and T_L is the load torque.

To consider the effect of magnetic saturation and spatial harmonics, λ_d, λ_q, and T_e are calculated as functions of i_d, i_q and rotor position θ_i as illustrated by (2). The relationships $\lambda_d(i_d, i_q, \theta_i)$, $\lambda_q(i_d, i_q, \theta_i)$, and T_e (i_d, i_q, θ_i) are calculated using the finite element analysis (FEA). These data are obtained via FEA by varying i_d from -20 to 0 A in steps of 1A, i_q is changed from from 0 to 20 A in steps of 1A, and θ_i is varied from 0˚ (d-axis) to 72˚ (q-axis for 12 slots, 10 poles IPMSM) insteps of 1˚ (mech. degree). Then, the average flux-linkages and torque are obtained according to (3). These results are shown in Figure 1 (a), Figure 1 (b), and Figure 1 (c). As noted, the flux linkages (λ_d, λ_q), and torque show nonlinear relations with currents (i_d, i_q). The stator pole shoes, and rotor rips have the highest flux densities. They are in deep saturation as illustrated by Figure 2.

$$\lambda_d = f\left(i_d, i_q, \theta_i\right), \quad \lambda_q = g\left(i_d, i_q, \theta_i\right), \quad T_e = T\left(i_d, i_q, \theta_i\right) \tag{2}$$

$$\lambda_d\left(i_d, i_q\right) = \frac{\sum_{i=0}^{N} \lambda_d(i_d, i_q, \theta_i)}{N+1}, \quad \lambda_q\left(i_d, i_q\right) = \frac{\sum_{i=0}^{N} \lambda_q(i_d, i_q, \theta_i)}{N+1}, \quad T_e\left(i_d, i_q\right) = \frac{\sum_{i=0}^{N} T_e(i_d, i_q, \theta_i)}{N+1} \tag{3}$$

By performing inverses of (3), i_d and i_q are determined by (4). The IPMSM model can be built as illustrated in Figure 3. The model is built based on (1)-(4). The inputs are the v_d and v_q. The voltages are employed to estimate λ_d and λ_q using (1). Then, armature currents (i_{da}, i_{qa}) are calculated using flux inverse model in (4). The iron losses are represented by currents i_{dfe} and i_{qfe}. The motor electromagnetic torque is estimated as a function of i_{da} and i_{qa} currents. Noting that the model involves not only magnetic saturation and spatial harmonic effects but also iron loss effect.

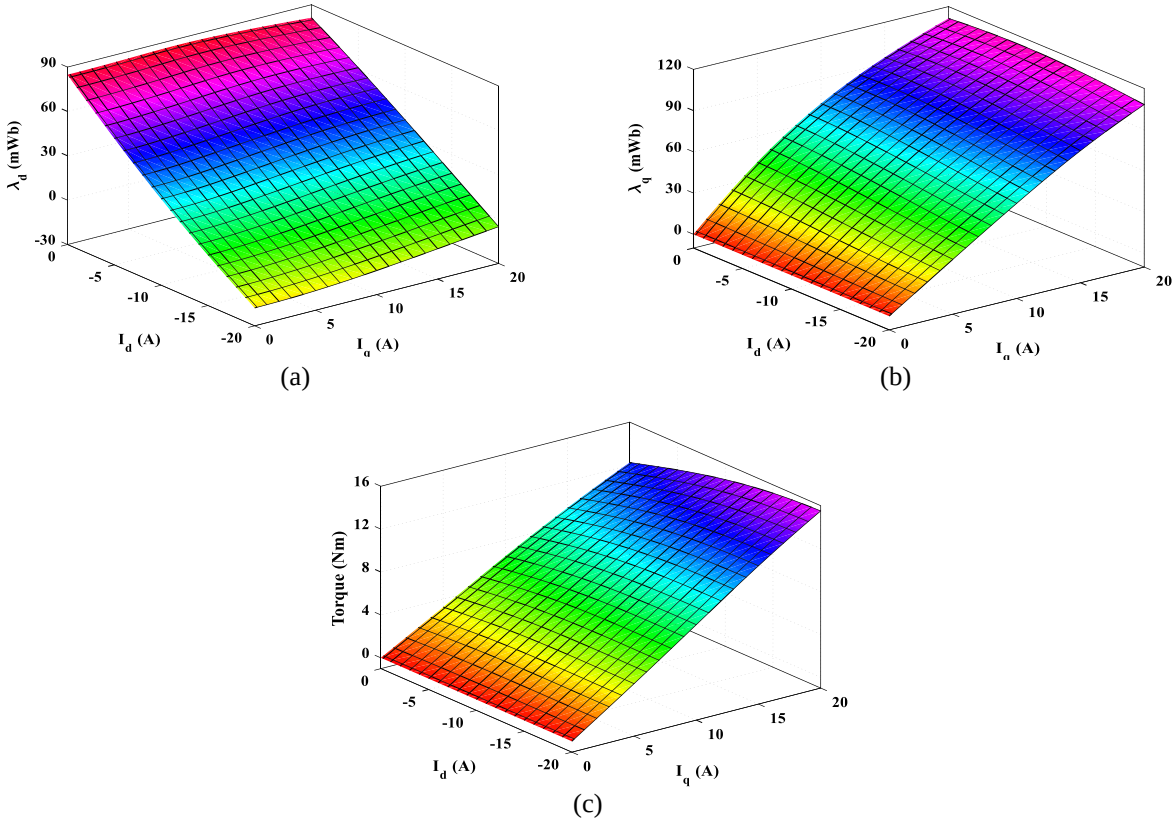

Figure 1. The FEA-calculated: (a) d-axis flux, (b) q-axis flux, (c) torque

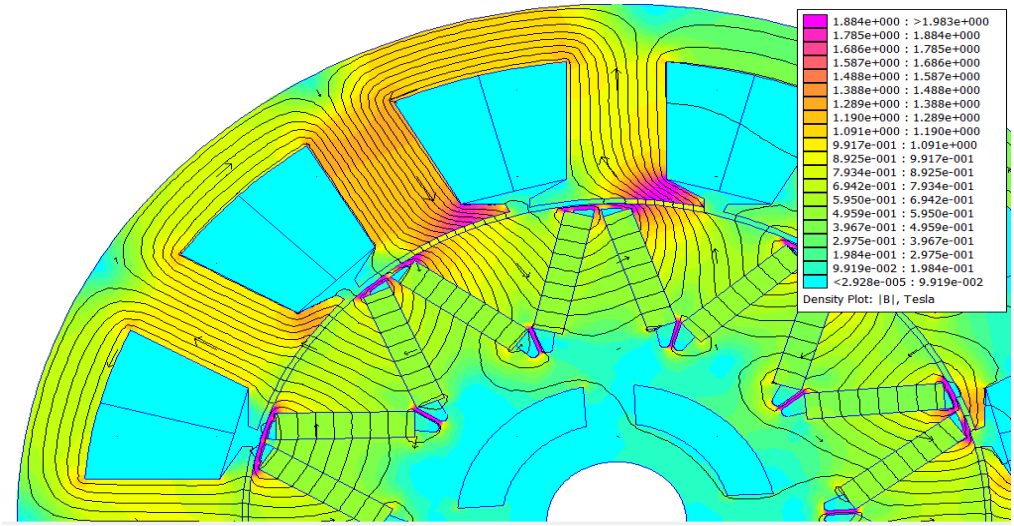

Figure 2. The flux lines and flux density at i_q=8A, i_d=-2A and θ_i= 0˚

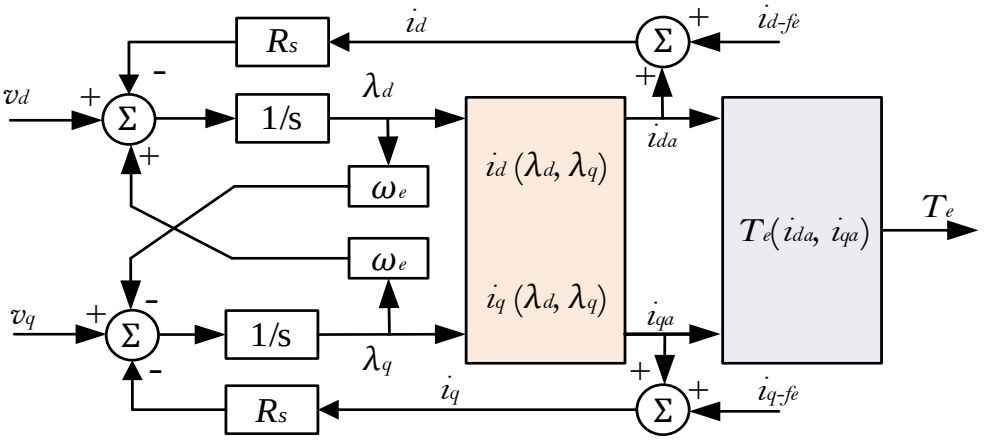

Figure 3. The schematic of IPMSM model

$$i_d = f^{-1}(\lambda_d, \lambda_q), \quad i_q = g^{-1}(\lambda_d, \lambda_q) \tag{4}$$

2.2. Loss modeling

This section describes the total system losses including motor and inverter losses. The total system losses (P_{loss}) are copper losses (P_{cu}), fundamental iron losses ($P_{Fe,f}$), harmonic iron losses ($P_{Fe,h}$), magnet loss (P_{Mag}), and inverter losses (P_{inv}). The total system losses (P_{loss}) are given by (5).

$$P_{loss} = P_{cu} + P_{Fe,f} + P_{Fe,h} + P_{Mag} + P_{inv} \tag{5}$$

2.2.1. Copper losses

The fundamental copper loss of an IPMSM can be estimated by (6). The harmonics copper losses can be ignored as the employed switching frequency of inverter is 10kHz [16].

$$P_{cu} = 3I_s^2 R_s = \frac{3}{2} R_s (i_d^2 + i_q^2) \tag{6}$$

2.2.2. Iron losses

The Bertotti iron loss formula is a widely used method to evaluate the iron loss in electric machines. It calculates iron losses per unit volume is being as [23].

$$P_{fe} = k_1(\lambda_d^2 + \lambda_q^2) + k_2(\lambda_d^{1.5} + \lambda_q^{1.5}), \quad k_1 = (k_h f + k_c f^2)\left(\frac{V_t}{A_{tc}^2} + \frac{V_y}{A_{yc}^2}\right), \quad k_2 = k_e f^{1.5}\left(\frac{V_t}{A_{tc}^{1.5}} + \frac{V_y}{A_{yc}^{1.5}}\right)$$

$$V_t = Q h_t A_t; \quad V_y = \pi(D_s - h_y)A_y; \quad k_c = \frac{\pi^2 \sigma k_d^2}{6}; \quad \phi_{d,q} = \frac{\sqrt{2}}{\sqrt{3}} \frac{\lambda_{d,q}}{N_T K_w} \tag{7}$$

$$A_{tc} = \frac{\sqrt{3}}{\sqrt{2}}(N_T K_w).\alpha_i A_t Q/(2p); \quad A_{yc} = \frac{\sqrt{3}}{\sqrt{2}}(N_T K_w).2A_y$$

where f is the frequency. The coefficients k_h, k_c, and k_e are for hysteresis, eddy current, and additional losses, respectively. V_t and V_y are the total volumes of stator tooth and yoke, respectively. The A_{tc} and A_{yc} are the equivalent areas of stator tooth and yoke, respectively. h_t and h_y are the heights of stator tooth and yoke, respectively. Q is the number of slots. A_t and A_y are the physical areas of stator tooth and yoke, respectively. D_s is the outer diameter of stator. σ is the material conductivity. k_d is the lamination thickness. N_T is the number of phase turns. K_w is the winding factor. ϕ_d and ϕ_q are the d- and q-axis fluxes. α_i is the pole arc factor. Without the consideration of excess loss, the equivalent iron loss resistance R_c is given as $R_c = \omega_e^2/k_1$.

2.2.3. The harmonic iron loss

It is calculated as a function of ripple voltage rms, ΔV_{rms}^2, DC link voltage V_{dc}, and modulation index m as given by (8) [24]. The modulation index is defined as $m = \frac{\sqrt{3}V_m}{V_{dc}}$.

$$P_{fe,h} = K_{h,eddy}\Delta V_{rms}^2; \quad where\ \Delta V_{rms}^2 = \frac{V_{dc}^2}{3}\left(\frac{2}{\pi}m - \frac{1}{2}m^2\right) \tag{8}$$

where V_m is the peak output voltage. $K_{h,\text{ eddy}}$ is the eddy current loss coefficient, it is taken as 2.3mW/V^2 [24].

2.2.4. The magnet loss

The magnet loss depends on magnet volume (V_M), magnet width (b_M), magnet resistivity (ρ_M), and the maximum value of flux density (B_m).

$$P_{mag} = \frac{V_M\, b_M^2 B_m^2 f^2}{12\rho_M} \tag{9}$$

2.2.5. The inverter losses

The inverter has both conduction and switching losses [25]. The conduction loss of one insulated gate bipolar transistor (IGBT) ($P_{co\text{-}IGBT}$) and conduction loss for one diode ($P_{co\text{-}diode}$) in a 2-level VSI can be defined by (10). Besides, the switching losses of one IGBT ($P_{SW\text{-}IGBT}$) and switching loss for one diode ($P_{SW\text{-}diode}$) in a 2-level VSI can be defined by (11) [26]. The total inverter losses (P_{inv}) can be estimated by (12).

$$\begin{aligned} P_{co\_IGBT} &= \frac{1}{2}\left(V_{ceo}\frac{I_m}{\pi} + R_o\frac{I_m^2}{4}\right) + m\cos\theta\left(V_{ceo}\frac{I_m}{8} + R_o\frac{I_m^2}{3\pi}\right) \\ P_{co\_diode} &= \frac{1}{2}\left(V_{Do}\frac{I_m}{\pi} + R_D\frac{I_m^2}{4}\right) - m\cos\theta\left(V_{Do}\frac{I_m}{8} + R_D\frac{I_m^2}{3\pi}\right) \end{aligned} \tag{10}$$

$$P_{SW-IGBT} = \frac{1}{\pi}(e_{on} + e_{off})f_s\left(\frac{V_{dc}}{V_{nom}}\right)\left(\frac{I_m}{I_{nom}}\right); \quad P_{SW-diode} = \frac{1}{\pi}e_{rr}f_s\left(\frac{V_{dc}}{V_{nom}}\right)\left(\frac{I_m}{I_{nom}}\right) \tag{11}$$

$$P_{inv} = 6 * \left((P_{co-IGBT} + P_{co-diode}) + (P_{SW-IGBT} + P_{SW-diode})\right) \tag{12}$$

where $cos\theta$ is the power factor, V_{ceo} and V_{Do} depict the threshold voltages for IGBT and diode, respectively, R_o and R_D represent the resistances of IGBT and diode, respectively, f_s is the switching frequency, e_{on} and e_{off} are the required amount of energy to turn-on and turn-off the IGBT, respectively, e_{rr} is the required amount of energy to turn-off the diode, I_m is the peak magnitude of current, V_{nom} and I_{nom} are the nominal voltage and current of loss measurements, respectively.

3. THE PROPOSED ONLINE EFFICIENCY OPTIMIZATION METHOD

The proposed OMEPA control determines the current angle (β) that maximizes the system efficiency. The flowchart of searching algorithm is illustrated in Figure 4. The procedure is achieved online for a known maximum current (I_m), and motor speed (ω). For each operating point, the current angle is changed in small steps ($\Delta\beta$). The d- and q-axis current components are estimated by (13). Then, the total system losses (P_{loss}) are estimated using (5)-(12). After that, the system efficiency (η) is updated by (13) considering the voltage and current constraints in (14). The online efficiency calculation should also consider the variations in temperature, DC voltage, and motor parameters.

- Measure DC voltage (V_{dc}), speed (ω), and temperature.
- The winding resistance is updated as a function of temperature using (15).
- For each current angle β, the d- and q-axis current components are calculated using (13).
- The d- and q-axis flux linkages are updated using (16).
- The d- and q-axis voltage components are updated using (17).
- The system losses are estimated using (5)-(12).
- The online system efficiency is updated using (13) considering the voltage and current constraints in (14).
- If $\beta \geq \beta_{\max}$, determine angle that corresponds to maximum efficiency. Else, β is changed by $\Delta\beta$, then go to point 2.

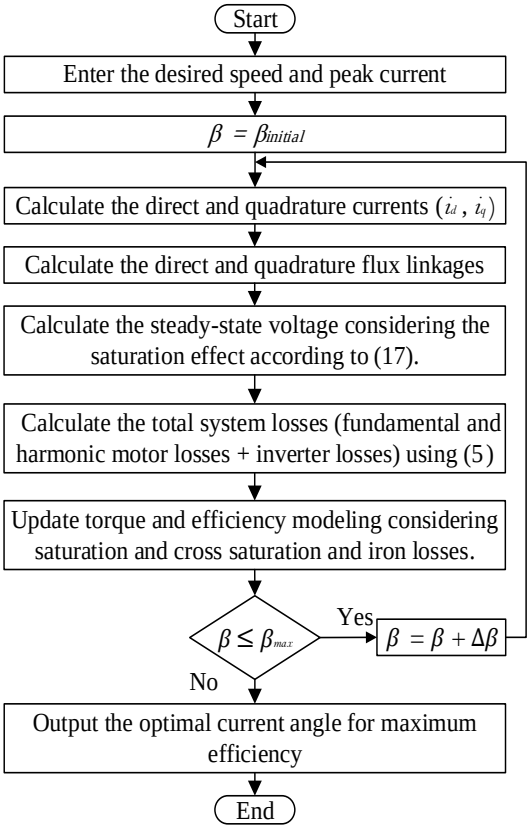

Figure 4. The Flowchart of searching algorithm

The temperature directly affects the stator resistance and hence the amount of copper loses. The temperature effect is included considering (15). The DC voltage is measured instantaneously each sample time. The motor parameters are fitted as functions of d-and q-axis current components. At each operating point, defined by ω and I_m, β angle corresponding to maximum efficiency is reported.

$$i_d = -I_m \sin\beta; \quad i_q = I_m \cos\beta; \quad \eta = \frac{T_e * \omega}{T_e * \omega + P_{loss}}; \tag{13}$$

$$\sqrt{V_d^2 + V_q^2} \leq V_{max}; \quad \sqrt{i_d^2 + i_q^2} \leq I_{max} \tag{14}$$

$$R = R_o\{1 + \alpha(T - T_o)\} \tag{15}$$

$$\lambda_d(i_d, i_q) = L_d(i_d, i_q) i_d + \lambda_{pm}(i_q); \quad \lambda_q(i_d, i_q) = L_q(i_d, i_q) i_q \tag{16}$$

$$v_d(i_d, i_q) = R i_d - \omega_e \lambda_q(i_d, i_q); \quad v_q(i_d, i_q) = R i_q + \omega_e \lambda_d(i_d, i_q) \tag{17}$$

where V_{max} and I_{max} are the maximum permissible phase voltage and phase current, respectively. R_o depicts the winding resistance at temperature T_o. T is the present temperature of windings. α is the thermal coefficient of copper. L_d and L_q are d- axis and q- axis inductances. λ_{PM} is the PM flux linkage.

4. RESULTS AND DISSCUSSION

The results include a steady state comparison between proposed OMEPA control method and offline maximum efficiency per ampere-lookup table (MEPA-LUT) control method reported in Ni *et al* [18]. Moreover, the dynamic behavior of OMEPA is presented and analyzed. The influence of DC voltage variation, temperature variation, and the variation of motor parameters is also investigated.

4.1. The steady state comparision

It is worthy noted that, the MEPA-LUT has an inherited capability to accurately determine the system efficiency as it runs motor model at each change in current angle (β). It also considers the update of reference voltages after the PI controller which improves the estimation of system losses. However, this method considers certain operating conditions. Any change of theses condition could lead to unaccepted performance. If the proposed OMEPA method can produce a high efficiency as MEPA-LUT control method, this means one thing that the proposed OMEPA can accurately estimate the system efficiency without the need to run motor model. It updates the flux and voltages after the variation of β using (16), (17).

Figure 5 (a), and Figure 5 (b) shows the steady state comparison between proposed OMEPA and conventional MEPA-LUT methods under two speeds of 1000 and 1750r/min, respectively. for each speed (1000 and 1750r/min), the maximum current is changed from 2A to 12A. Then, the best current angle is defined by each control method (OMEPA and MEPA-LUT). After that, the corresponding system efficiencies are calculated and compared. As noted, the two efficiencies are very close. This in turn verifies the calculation accuracy of system efficiency using the proposed OMEPA. The lower part of Figure 5 shows efficiency error (η_{Error}). This error is defined by $\eta_{Error} = \eta_{OMEPA} - \eta_{MEPA\text{-}LUT}$. Positive error means higher system efficiency by the proposed OMEPA and vice versa. As noted, the efficiency error (η_{Error}) is almost positive despite its small values. This happens because the proposed OMEPA method could search with smaller angle resolutions ($\Delta\beta$) compared to MEPA-LUT method.

4.2. The dynamic performance of proposed OMEPA during payload Torque change

Figure 6 shows the dynamic performance of the proposed OMEPA under sudden changes in load torque at the rated speed of 1500r/min. The load is changes as illustrated by Figure 6 (a). As a result, the maximum current (I_m) is also changing correspondingly with load torque see Figure 6 (b). The proposed OMEPA determines the best current angle (β) that corresponding to maximum efficiency see Figure 6 (c). As noted, the proposed OMEPA updates β each control period which reflects the fast dynamic performance in Figure 6 (c). The variation of β also varies both the d- and q-axis current as shown in Figure 6 (d), Figure 6 (e), respectively. Theses affects the system losses and hence the system efficiency as seen in Figure 6 (f).

4.3. Effect of DC voltage variation

In most EVs, the battery voltage (DC voltage) changes depending on its state of charge (SOC). The voltage variation affects system performance especially at high speeds. Figure 7 shows the simulation results under variation of DC voltage at 2000r/min. The DC voltage is changed from 200V (rated voltage) to 170V at 0.1sec. As seen in Figure 7 (a), Figure 7 (b) and Figure 7 (c), for the convention MEPA-LUT method, from 0 to 0.1sec, the system tracks accurately the commanded reference currents and produces the required torque under the rated voltage. When the voltage decreases to 170V at 0.1sec, the system fails to track the currents and hence fails to produce the required torque. This happens because the LUT are generated under rated voltage of 200V and does not consider voltage variations. Hence, the reference d-and q-axis currents need to be corrected with the variation of DC voltage. On the contrary, for the proposed OMEPA method, the system tracks accurately the commanded reference current despite voltage variations, it also produces the required torque Figure 7 (d), Figure 7 (e) and Figure 8 (f).

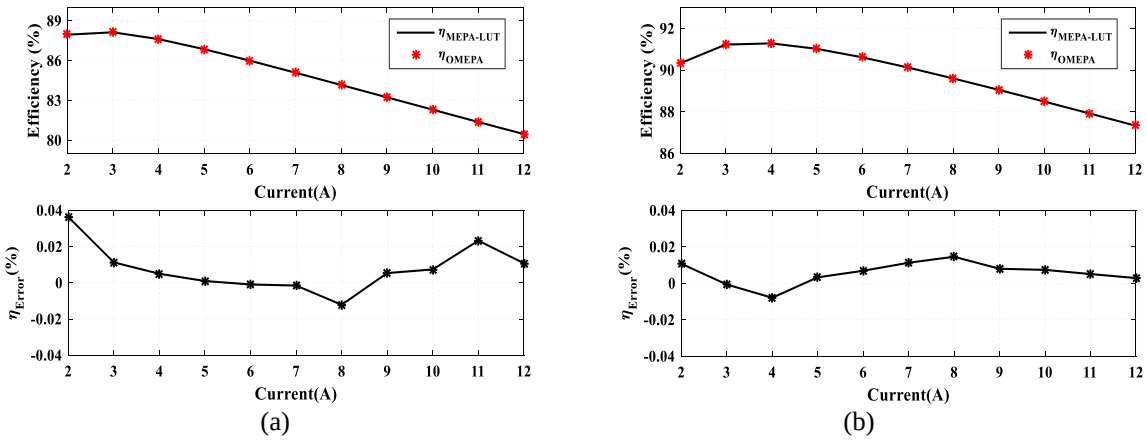

Figure 5. Comparative between OMEPA and MEPA-LUT at, (a)1000 r/min, and (b) 1750 r/min

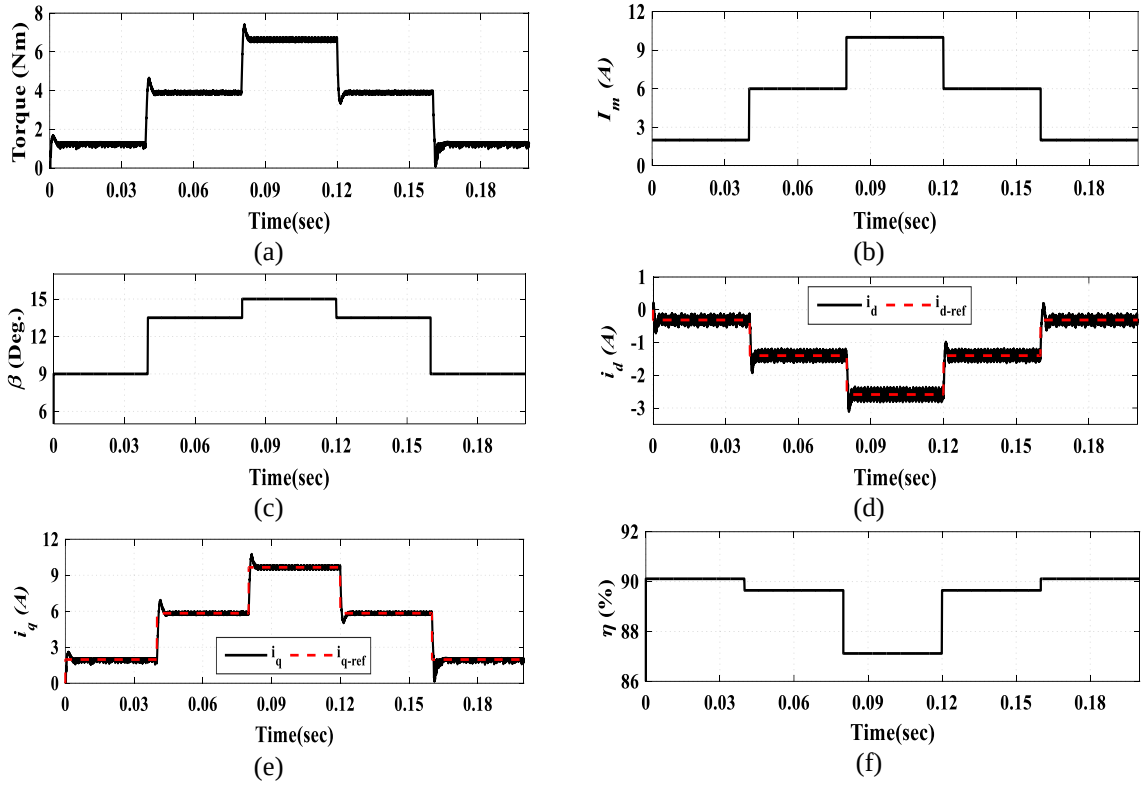

Figure 6. Simulation results of OMEPA during torque changing, (a) the electromagnetic torque, (b) the maximum current, (c) the current angle, (d) the d-axis currents, (e) the d-axis currents, (f) the system efficiency

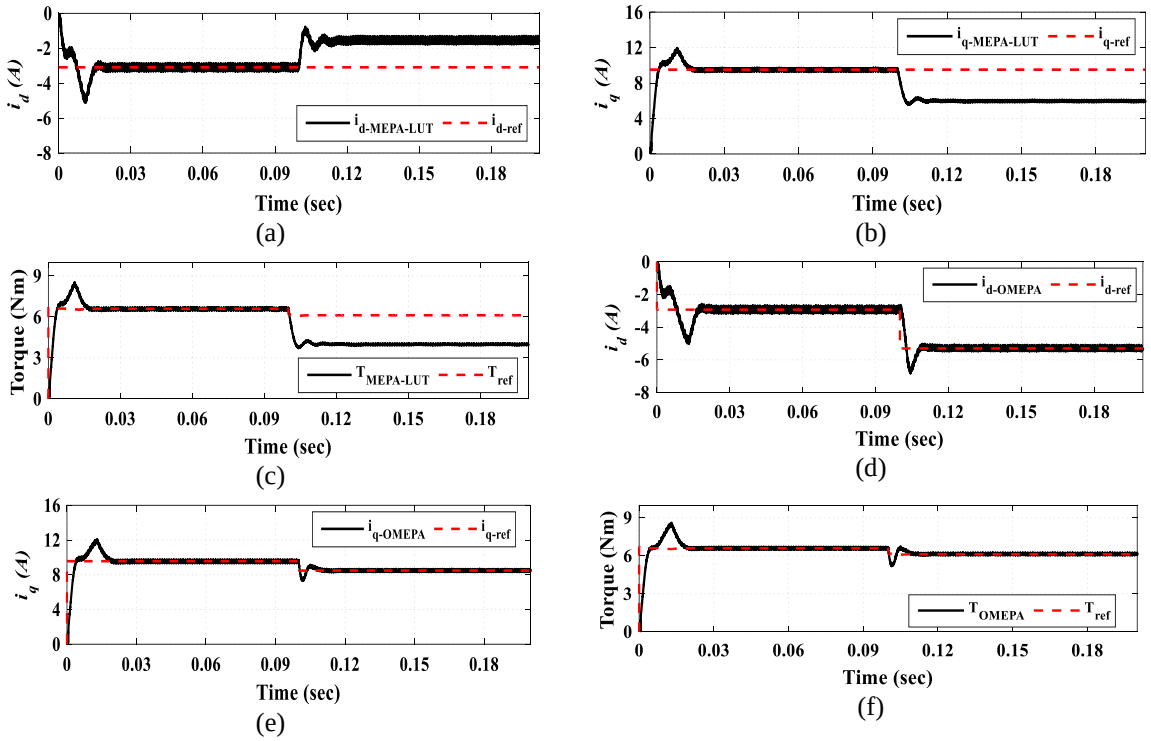

Figure 7. Simulation results under variation of DC voltage at 2000r/min, (e) q-axis currents with OMEPA, (f) Torque with OMEPA

4.4. Effect of temperature and motor parameter variations

The IPMSMs in EVs have temperature sensors that are installed in stator windings. These sensors provide instantaneous temperature variations not only for protection issues but also for control ones. The winding resistance of IPMSM changes with the temperature as illustrated by (15). The change of stator resistance will affect the amount of copper losses. Hence, it affects the accuracy of efficiency calculation for both the online and offline calculations.

The offline MEPA control methods assumes constant stator resistance. When the temperature increases, the resistance will also increase, and hence the copper losses. Therefore, the offline MEPA method will deviate from the MEPA operation. In order to include the effect of temperature within the offline MEPA control, several experimental measurements are required which means cost, effort, and time. On the contrary, once the temperature is measured by the temperature sensors, the stator resistance is updated using (15) within the control algorithm of the proposed OMEPA. This is a very simple implementation method that compensates for the resistance variation due to the temperature.

Figure 8 (a), and Figure 8 (b) shows the effect of temperature on both copper loss and efficiency, respectively. The amount of copper losses considering temperature effect ($P_{cu\text{-}CTE}$) is greater than that without considering temperature effect ($P_{cu\text{-}WCTE}$) as illustrated by Figure 8 (a). The corresponding system efficiency at 10A is shown in Figure 8 (b), as seen, the proposed OMEPA has higher system efficiency as it considers the real amount of copper losses due to temperature variations. If the motor parameters changes, they can be considered within the control algorithm of OMEPA by the same way the temperature is considered. Online parameter estimation methods can be used to estimate the accurate motor parameters, then, theses parameters can be used very simply within the OMEPA control.

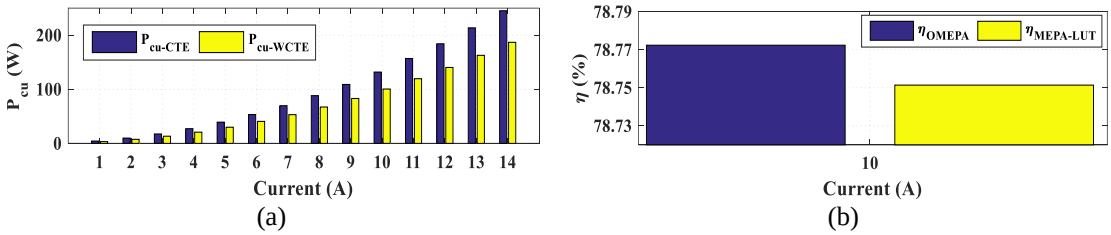

Figure 8. Effect of temperature variation on copper losses and efficiency, (a) copper losses, and (b) system efficiency at 1000r/min and at 100^0C

5. CONCLUSION

An online maximum efficiency control method for IPMSM in EVs is introduced in this paper. The system efficiency is calculated online based on the detailed system loss models. A searching algorithm for the current angle that corresponds to maximum efficiency point is developed. The proposed OMEPA control offers high dynamic performance as it updates the current angle at each control period. It also offers higher flexibility as it can consider any instantaneous variations of DC voltage (battery voltage), temperature, and motor parameters. The proposed OMEPA control method is independent in tracking the maximum efficiency point as well as robust to DC voltage variations.

REFERENCES

[1] F. Aymen, M. Alowaidi, M. Bajaj, N. K. Sharma, S. Mishra, and S. K. Sharma, "Electric vehicle model based on multiple recharge system and a particular traction motor conception," *IEEE Access*, vol. 9, pp. 49308-49324, 2021, doi: 10.1109/ACCESS.2021.3068262.

[2] L. Dang, N. Bernard, N. Bracikowski, and G. Berthiau, "Design optimization with flux weakening of high-speed PMSM for electrical vehicle considering the driving cycle," *IEEE Transactions on Industrial Electronics*, vol. 64, no. 12, pp. 9834-9843, Dec. 2017, doi: 10.1109/TIE.2017.2726962.

[3] A. Flah, M. Novak, and S. Lassaad, "An improved reactive power MRAS speed estimator with optimization for a hybrid electric vehicles application," *ASME, Journal of Dynamic Systems, Measurement, and Control*, vol. 140, no. 6, p. 061016, 2018, doi: 10.1115/1.4039212.

[4] X. Chen, "Modelling and design of permanent-magnet machines for electric vehicle traction," thesis, Department of Electronic and Electrical Engineering, The University of Sheffield, 2015.

[5] C. T. Krasopoulos, M. E. Beniakar, and A. G. Kladas, "Multicriteria PM motor design based on ANFIS evaluation of EV driving cycle efficiency," *IEEE Transactions on Transportation Electrification*, vol. 4, no. 2, pp. 525-535, June 2018, doi: 10.1109/TTE.2018.2810707.

[6] A. Flah and L. Sbita, "Overview on BLAC and BLDC motors: designs and mathematical modeling," *International Journal of Powertrains*, vol. 9, no. 5, pp. 239-243, 2021.

[7] H. Hanene, A. Flah, and T. Souhir, "Variable reluctance synchronous machines in saturated mode," *International Journal of Power Electronics and Drive Systems (IJPEDS)*, vol. 12, no. 2, pp. 662-673 June 2021, doi: 10.11591/ijpeds.v12.i2.pp662-673.
[8] C. Lu, S. Ferrari, and G. Pellegrino, "Two design procedures for PM synchronous machines for electric powertrains," *IEEE Transactions on Transportation Electrification*, vol. 3, no. 1, pp. 98-107, March 2017, doi: 10.1109/TTE.2016.2646738.
[9] J. Wu, J. Wang, C. Gan, Q. Sun, and W. Kong, "Efficiency optimization of PMSM drives using field-circuit coupled FEM for EV/HEV applications," *IEEE Access*, vol. 6, pp. 15192-15201, 2018, doi: 10.1109/ACCESS.2018.2813987.
[10] W. Deng, Y. Zhao, and J. Wu, "Energy efficiency improvement via bus voltage control of inverter for electric vehicles," *IEEE Transactions on Vehicular Technology*, vol. 66, no. 2, pp. 1063-1073, Feb. 2017, doi: 10.1109/TVT.2016.2555990.
[11] J. O. Estima and A. J. M. Cardoso, "Efficiency analysis of drive train topologies applied to electric/hybrid vehicles," *IEEE Transactions on Vehicular Technology*, vol. 61, no. 3, pp. 1021-1031, March 2012, doi: 10.1109/TVT.2012.2186993.
[12] X. Zhou, Y. Zhou, H. Wang, M. Lu, F. Zeng, and Y. Yu, "An improved MTPA control based on amplitude-adjustable square wave injection," *IEEE Transactions on Energy Conversion*, vol. 35, no. 2, pp. 956-965, June 2020, doi: 10.1109/TEC.2020.2968737.
[13] C. Lai, G. Feng, K. Mukherjee, J. Tjong and N. C. Kar, "Maximum torque per ampere control for IPMSM using gradient descent algorithm based on measured speed harmonics," *IEEE Transactions on Industrial Informatics*, vol. 14, no. 4, pp. 1424-1435, April 2018, doi: 10.1109/TII.2017.2759812.
[14] K. Li and Y. Wang, "Maximum torque per ampere (MTPA) control for IPMSM drives based on a variable-equivalent-parameter MTPA control law," *IEEE Transactions on Power Electronics*, vol. 34, no. 7, pp. 7092-7102, July 2019, doi: 10.1109/TPEL.2018.2877740.
[15] H. Wang, C. Li, G. Zhang, Q. Geng, and T. Shi, "Maximum torque per ampere (MTPA) control of IPMSM systems based on controller parameters self-modification," *IEEE Transactions on Vehicular Technology*, vol. 69, no. 3, pp. 2613-2620, March 2020, doi: 10.1109/TVT.2020.2968133.
[16] A. Balamurali, G. Feng, A. Kundu, H. Dhulipati and N. C. Kar, "Noninvasive and improved torque and efficiency calculation toward current advance angle determination for maximum efficiency control of PMSM," *IEEE Transactions on Transportation Electrification*, vol. 6, no. 1, pp. 28-40, March 2020, doi: 10.1109/TTE.2019.2962333.
[17] A. Balamurali, G. Feng, C. Lai, J. Tjong, and N. C. Kar, "Maximum efficiency control of PMSM drives considering system losses using gradient descent algorithm based on DC power measurement," *IEEE Transactions on Energy Conversion*, vol. 33, no. 4, pp. 2240-2249, Dec. 2018, doi: 10.1109/TEC.2018.2852219.
[18] R. Ni, D. Xu, G. Wang, L. Ding, G. Zhang, and L. Qu, "Maximum efficiency per ampere control of permanent-magnet synchronous machines," *IEEE Transactions on Industrial Electronics*, vol. 62, no. 4, pp. 2135-2143, April 2015, doi: 10.1109/TIE.2014.2354238.
[19] M. N. Uddin and R. S. Rebeiro, "Online efficiency optimization of a fuzzy-logic-controller-based IPMSM drive," *IEEE Transactions on Industry Applications*, vol. 47, no. 2, pp. 1043-1050, March-April 2011, doi: 10.1109/TIA.2010.2103293.
[20] S. Yang, K. Liu, Y. Hu, L. Chu and S. Chen, "Efficiency optimization control of IPMSM considering varying machine parameters," in *2018 IEEE Student Conference on Electric Machines and Systems*, 2018, pp. 1-6, doi: 10.1109/SCEMS.2018.8624761.
[21] M. Li, S. Huang, X. Wu, K. Liu, X. Peng, and G. Liang, "A virtual HF signal injection based maximum efficiency per ampere tracking control for IPMSM drive," *IEEE Transactions on Power Electronics*, vol. 35, no. 6, pp. 6102-6113, June 2020, doi: 10.1109/TPEL.2019.2951754.
[22] H. Kim, Y. Lee, S. Sul, J. Yu, and J. Oh, "Online MTPA control of IPMSM based on robust numerical optimization technique," *IEEE Transactions on Industry Applications*, vol. 55, no. 4, pp. 3736-3746, July-Aug. 2019, doi: 10.1109/TIA.2019.2904567.
[23] D. Lin, P. Zhou, W. N. Fu, Z. Badics, and Z. J. Cendes, "A dynamic core loss model for soft ferromagnetic and power ferrite materials in transient finite element analysis," *IEEE Transactions on Magnetics*, vol. 40, no. 2, pp. 1318-1321, March 2004, doi: 10.1109/TMAG.2004.825025.
[24] M. Schweizer, T. Friedli, and J. W. Kolar, "Comparative evaluation of advanced three-phase three-level inverter/converter topologies against two-level systems," *IEEE Transactions on Industrial Electronics*, vol. 60, no. 12, pp. 5515-5527, Dec. 2013, doi: 10.1109/TIE.2012.2233698.
[25] M. Saur, B. Piepenbreier, W. Xu, and R. D. Lorenz, "Implementation and evaluation of inverter loss modeling as part of DB-DTFC for loss minimization each switching period," in *2014 16th European Conference on Power Electronics and Applications*, 2014, pp. 1-10, doi: 10.1109/EPE.2014.6910691.
[26] J. Guo, "Modeling and design of inverters using novel power loss calculation and dc-link current/voltage ripple estimation methods and bus bar analysis," Ph.D. dissertation, Electrical and Computer Engineering, McMaster University, 2017.